

Spin Current and Current-Induced Spin Transfer Torque in Ferromagnet-Quantum Dot-Ferromagnet Coupled Systems

Hai-Feng Mu, Gang Su*, and Qing-Rong Zheng

*College of Physical Sciences, Graduate University of Chinese Academy of Sciences,
P.O. Box 4588, Beijing 100049, China*

Abstract

Based on Keldysh's nonequilibrium Green function method, the spin-dependent transport properties in a ferromagnet-quantum dot (QD)-ferromagnet coupled system are investigated. It is shown the spin current shows quite different characteristics from its electrical counterpart, and by changing the relative orientation of both magnetizations, it can change its magnitude even sign. The current-induced spin transfer torque (CISTT) is uncovered to be greatly enhanced when the bias voltage meets with the discrete levels of the QD at resonant positions. The relationship between the CISTT, the electrical current and the spin current is also addressed.

PACS numbers: 75.47.-m, 73.63.Kv, 75.70.Cn

I. INTRODUCTION

Investigations on the spin-dependent transport in a magnetic tunnel junction (MTJ) have attracted much interest in the last decade, as the MTJs have essential applications in spintronic devices[1, 2, 3, 4, 5]. One of phenomena in MTJs is the so-called tunnel magnetoresistance (TMR) effect, which states that the tunneling current through the junction depends sensitively on the relative orientation of the magnetizations of both ferromagnetic electrodes, that is caused by the spin-dependent scattering of conduction electrons. The difference between the currents through spin up and down channels in MTJs is usually referred to as the spin current[4]. On the other hand, a reverse effect to TMR was predicted independently by Slonczewski[6] and Berger[7], i.e., the spin-polarized electrons passing from the left ferromagnetic layer into the right layer in which the magnetization deviates the left by an angle may exert a torque to the right ferromagnet and can change the orientation of its magnetization. This effect was coined as the spin transfer effect (for review, see e.g. Ref.[5, 8]), which can lead to the current-induced magnetization reversal, and might offer a promise for the current-controlled spintronic devices. It has recently attracted intensive investigations both experimentally[9, 10, 11, 12, 13, 14] and theoretically[15, 16, 17, 18, 19, 20, 21, 22].

Among other magnetic tunnel structures (e.g. Refs.[23]), the ferromagnet-quantum dot-ferromagnet (FM-QD-FM) coupled systems have also received much attention recently. Previous theoretical works on spin-dependent transport through QDs are mainly focused on the tunnel electrical current and the TMR effect for collinear configuration[24, 25, 26, 27, 28, 29, 30] and noncollinear configuration[31, 32, 33, 34, 35, 36, 37, 38, 39]. However, the investigations on the spin current and the current-induced spin transfer torque (CISTT) in such systems are sparsely reported. It is the purpose of this paper to study the spin current and spin transfer torque in FM-QD-FM coupled MTJs.

In terms of Keldysh's nonequilibrium Green function method, the tunnel electrical current, the spin current and the spin transfer torque in the FM-QD-FM coupled system will be investigated. It is found the spin current exhibits different behaviors from its electrical counterpart. It is also shown that the resonant positions for the tunneling electrical current and spin current become far separated with the increase of the Coulomb interaction U in the QD. The magnitudes of the CISTT at two resonant positions are found to be greatly enhanced at resonant positions. At the bias larger than $(\varepsilon_0 + U)/e$, the CISTT can reach

a saturation plateau which is independent of the Coulomb interaction. The CISTT shows a kink-like behavior with the increase of the spin current. The relationship between the CISTT, the electrical current and the spin current is also addressed.

The rest of this paper is outlined as follows. In Sec. II, the model and formalism for the tunnel electrical current, the spin current and the current-induced spin transfer torque will be established. In Sec. III, the corresponding numerical results will be given. Finally, a summary will be presented.

II. MODEL AND FORMALISM

Let us consider a single-level QD coupled to two ferromagnetic electrodes. The left (L) and right (R) electrodes are connected with the bias voltage $V/2$ and $-V/2$, respectively, as shown in Fig. 1. The magnetic moment \mathbf{M}_L of the left FM is assumed to be parallel to the z axis, while the moment \mathbf{M}_R of the right FM is aligned along the z' axis which deviates the z axis by a relative angle θ . The tunnel current flows along the x axis and perpendicular to the junction plane. The system consists of the left, right, QD and coupling parts, and can be described by the following Hamiltonian:

$$H = H_L + H_R + H_d + H_T, \quad (1)$$

with

$$H_L = \sum_{k\sigma} \varepsilon_{kL\sigma} a_{kL\sigma}^\dagger a_{kL\sigma}, \quad (2)$$

$$H_R = \sum_{k\sigma} [\varepsilon_R(k) - \sigma \mathbf{M}_R \cos \theta] a_{kR\sigma}^\dagger a_{kR\sigma} - \mathbf{M}_R \sin \theta a_{kR\sigma}^\dagger a_{kR\bar{\sigma}}, \quad (3)$$

$$H_d = \sum_{\sigma} \varepsilon_0 c_{\sigma}^\dagger c_{\sigma} + U n_{\uparrow} n_{\downarrow}, \quad (4)$$

$$H_T = \sum_{k\alpha\sigma} T_{k\alpha} a_{k\alpha\sigma}^\dagger c_{\sigma} + h.c., \quad \alpha = L, R. \quad (5)$$

where $\varepsilon_{k\alpha\sigma} = \varepsilon_{\alpha}(k) - \sigma \mathbf{M}_{\alpha} - eV_{\alpha}$ is the single-electron energy for the wavevector \mathbf{k} and spin σ in the α electrode, $a_{k\alpha\sigma}$ and c_{σ} are annihilation operators of electrons with spin σ in the α electrode and the QD, respectively, $n_{\sigma} = c_{\sigma}^\dagger c_{\sigma}$, U represents the on-site Coulomb

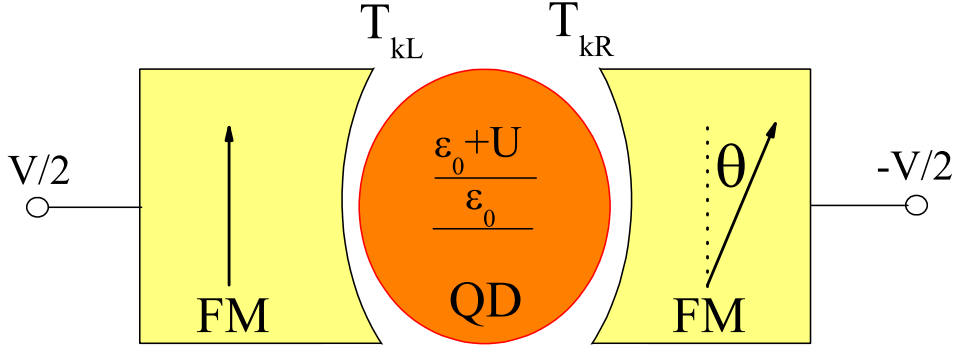


FIG. 1: Schematic illustration of the system consisting of two ferromagnets and a quantum dot separated by the tunnel barriers, where $T_{k\alpha}$ ($\alpha = L, R$) stands for the coupling matrix between the α electrode and the QD, and both magnetizations are aligned by a relative angle θ .

interaction between electrons in the QD, and $T_{k\alpha}$ is the coupling matrix elements between the α electrode and the QD.

A. Tunnel electrical current and spin current

The tunnel electrical current is composed of the sum of the currents carried by spin up and down electrons:

$$I(V) = I_{L\uparrow}(V) + I_{L\downarrow}(V), \quad (6)$$

while the spin current is defined by the difference between the electrical currents through the spin up and down channels[4]:

$$I_s(V) = I_{L\uparrow}(V) - I_{L\downarrow}(V), \quad (7)$$

where

$$I_{L\uparrow}(V) = -\frac{2e}{\hbar} \Re e \sum_{kL} T_{kL} G_{kL}^{\uparrow\uparrow, <}(t, t),$$

$$I_{L\downarrow}(V) = -\frac{2e}{\hbar} \Re e \sum_{kL} T_{kL} G_{kL}^{\downarrow\downarrow, <}(t, t).$$

with $G_{kL}^{\sigma'\sigma, <}(t, t') = i \langle a_{kL\sigma}^\dagger(t') c_{\sigma'}(t) \rangle$ the lesser Green function.

By applying the Langrenth theorem and Fourier transform, we may obtain the following equation

$$G_{kL}^<(\varepsilon) = T_{kL}^*[G^r(\varepsilon)g_{kL}^<(\varepsilon) + G^<(\varepsilon)g_{kL}^a(\varepsilon)], \quad (8)$$

where $G_{k\alpha}^{r,<}(\varepsilon) = \begin{pmatrix} G_{k\alpha}^{\uparrow\uparrow r,<}(\varepsilon) & G_{k\alpha}^{\uparrow\downarrow r,<}(\varepsilon) \\ G_{k\alpha}^{\downarrow\uparrow r,<}(\varepsilon) & G_{k\alpha}^{\downarrow\downarrow r,<}(\varepsilon) \end{pmatrix}$, $G^{r,<}(\varepsilon) = \begin{pmatrix} G^{\uparrow\uparrow r,<}(\varepsilon) & G^{\uparrow\downarrow r,<}(\varepsilon) \\ G^{\downarrow\uparrow r,<}(\varepsilon) & G^{\downarrow\downarrow r,<}(\varepsilon) \end{pmatrix}$, $g_{k\alpha}^<(\varepsilon) = \begin{pmatrix} i2\pi f_\alpha(\varepsilon_{k\alpha\uparrow})\delta(\varepsilon - \varepsilon_{k\alpha\uparrow}) \\ i2\pi f_\alpha(\varepsilon_{k\alpha\downarrow})\delta(\varepsilon - \varepsilon_{k\alpha\downarrow}) \end{pmatrix}$, $g_{k\alpha}^{r,a}(\varepsilon) = \begin{pmatrix} \frac{1}{\varepsilon - \varepsilon_{k\alpha\uparrow} \pm i\eta} \\ \frac{1}{\varepsilon - \varepsilon_{k\alpha\downarrow} \pm i\eta} \end{pmatrix}$, $G^r(\varepsilon)$ and $G^<(\varepsilon)$ are the retarded and lesser Green functions of the QD, respectively, and $f_\alpha(\varepsilon)$ is the Fermi distribution function in the α electrode. By defining $M(\varepsilon) = [f_L(\varepsilon)(G^r(\varepsilon) - G^a(\varepsilon)) + G^<(\varepsilon)]\Gamma_L(\varepsilon)$, we can simplify $I_{\uparrow(\downarrow)}(V)$ as

$$I_{\uparrow(\downarrow)}(V) = -\frac{ie}{\hbar} \int \frac{d\varepsilon}{2\pi} M_{\uparrow\uparrow(\downarrow\downarrow)}(\varepsilon),$$

where $M = \begin{pmatrix} M_{\uparrow\uparrow} & M_{\uparrow\downarrow} \\ M_{\downarrow\uparrow} & M_{\downarrow\downarrow} \end{pmatrix}$ is a 2×2 matrix, $\Gamma_\alpha(\varepsilon) = \begin{pmatrix} \Gamma_{\alpha\uparrow}(\varepsilon) \\ \Gamma_{\alpha\downarrow}(\varepsilon) \end{pmatrix}$ with $\Gamma_{\alpha\sigma}(\varepsilon) = 2\pi \sum_{k\alpha} |T_{k\alpha}|^2 \delta(\varepsilon - \varepsilon_{k\alpha\sigma})$.

The lesser Green function $G^<$ can be calculated by the Keldysh equation $G^< = G^r \Sigma^< G^a$. To get $\Sigma^<$, we invoke Ng's ansatz[40]: $\Sigma^< = \Sigma_0^< B$, where $\Sigma_0^<(\varepsilon) = i[f_L(\varepsilon)\Gamma_L + f_R(\varepsilon)\mathcal{R}\Gamma_R\mathcal{R}^\dagger]$, $B = (\Sigma_0^r - \Sigma_0^a)^{-1}(\Sigma^r - \Sigma^a)$, $\Sigma_0^r(\varepsilon) - \Sigma_0^a(\varepsilon) = -i[\Gamma_L + \mathcal{R}\Gamma_R\mathcal{R}^\dagger]$, $\Sigma^r(\varepsilon) - \Sigma^a(\varepsilon) = G^{a-1} - G^{r-1}$, and $\mathcal{R} = \begin{pmatrix} \cos \frac{\theta}{2} & -\sin \frac{\theta}{2} \\ \sin \frac{\theta}{2} & \cos \frac{\theta}{2} \end{pmatrix}$. Under these considerations, we finally get

$$I_{\uparrow(\downarrow)}(V) = \frac{e}{\hbar} \int \frac{d\varepsilon}{2\pi} (f_R - f_L) X_{\uparrow\uparrow(\downarrow\downarrow)}. \quad (9)$$

where $X = G^r \mathcal{R} \Gamma_R \mathcal{R}^\dagger B G^a \Gamma_L = \begin{pmatrix} X_{\uparrow\uparrow} & X_{\uparrow\downarrow} \\ X_{\downarrow\uparrow} & X_{\downarrow\downarrow} \end{pmatrix}$ is also a 2×2 matrix.

Consequently, the tunnel current and spin current have the forms of

$$I(V) = \frac{e}{\hbar} \int \frac{d\varepsilon}{2\pi} (f_R - f_L) \text{Tr} X, \quad (10)$$

$$I_s(V) = \frac{e}{\hbar} \int \frac{d\varepsilon}{2\pi} (f_R - f_L) \text{Tr}(X \hat{\sigma}_3). \quad (11)$$

with $\hat{\sigma}_3 = \begin{pmatrix} 1 & 0 \\ 0 & -1 \end{pmatrix}$ the Pauli matrix.

B. Current-induced spin transfer torque

The spin torque exerting on the right ferromagnet is determined by the time evolution rate of the total spin in the right ferromagnet[6, 7], which is composed of two parts: one is caused by the spin-dependent potential that is known as the equilibrium torque, the other is the current-induced spin transfer torque caused by the tunnel Hamiltonian H_T . By means of the nonequilibrium Green functions, the CISTT exerting on the right ferromagnet can be obtained by[17]

$$\tau^{Rx'} = -\cos\theta\Re e \sum_{kR} \int \frac{d\varepsilon}{2\pi} Tr[G_{kR}^<(\varepsilon)\hat{\sigma}_1 T_{kR}^*] + \sin\theta\Re e \sum_{kR} \int \frac{d\varepsilon}{2\pi} Tr[G_{kR}^<(\varepsilon)\hat{\sigma}_3 T_{kR}^*], \quad (12)$$

where $\hat{\sigma}_1 = \begin{pmatrix} 0 & 1 \\ 1 & 0 \end{pmatrix}$.

By a treatment similar to Eq. (8), we can obtain

$$G_{kR}^<(\varepsilon) = T_{kR}[G^r(\varepsilon)\mathcal{R}g_{kR}^<(\varepsilon)\mathcal{R}^\dagger + G^<(\varepsilon)\mathcal{R}g_{kR}^a(\varepsilon)\mathcal{R}^\dagger].$$

Therefore, the CISTT can be rewritten as

$$\tau^{Rx'} = \frac{1}{4\pi} \int d\varepsilon (f_R - f_L) Tr[G^r(\varepsilon)\Gamma_L B G^a(\varepsilon)\mathcal{R}\Gamma_R \mathcal{R}^\dagger (-\cos\theta\hat{\sigma}_1 + \sin\theta\hat{\sigma}_3)]. \quad (13)$$

The remaining task is to calculate the retarded Green function G^r .

By the equation of motion, we can derive

$$(\varepsilon - \varepsilon_0)G^r(\varepsilon) = \mathbf{1} + \sum_{k\alpha} T_{k\alpha}^* G_{k\alpha}^r(\varepsilon) + U G^{(2)r}(\varepsilon), \quad (14)$$

where $\mathbf{1}$ is a unit matrix, $G^{(2)r}(\varepsilon) = \begin{pmatrix} G^{\uparrow\uparrow(2)r}(\varepsilon) & G^{\uparrow\downarrow(2)r}(\varepsilon) \\ G^{\downarrow\uparrow(2)r}(\varepsilon) & G^{\downarrow\downarrow(2)r}(\varepsilon) \end{pmatrix}$, $G_{k\alpha}^{\sigma'\sigma,r}(t-t') = -i\theta(t-t')\langle\{a_{k\alpha\sigma'}(t), c_\sigma^\dagger(t')\}\rangle$, $G^{\sigma'\sigma,(2)r}(t-t') = -i\theta(t-t')\langle\{c_{\sigma'}(t)n_{\bar{\sigma}'}(t), c_\sigma^\dagger(t')\}\rangle$, and

$$G_{kL}^r = T_{kL} g_{kL}^r G^r(\varepsilon),$$

$$G_{kR}^r = T_{kR} \mathcal{R} g_{kR}^r \mathcal{R}^\dagger G^r(\varepsilon).$$

Substituting these equations into Eq. (14), up to the third-order of Green functions, we arrive at

$$(\varepsilon - \varepsilon_0 - U)G^{(2)r}(\varepsilon) = N + \sum_{k\alpha} [T_{k\alpha}^* G_{k\alpha}^{1(2)r}(\varepsilon) + T_{k\alpha} G_{k\alpha}^{2(2)r}(\varepsilon) - T_{k\alpha}^* G_{k\alpha}^{3(2)r}(\varepsilon)], \quad (15)$$

$$\text{where } N = \begin{pmatrix} \langle n_{\downarrow} \rangle & -\langle c_{\downarrow}^{\dagger} c_{\uparrow} \rangle \\ -\langle c_{\uparrow}^{\dagger} c_{\downarrow} \rangle & \langle n_{\uparrow} \rangle \end{pmatrix}, \quad G_{k\alpha}^{i(2)r} = \begin{pmatrix} G_{k\alpha}^{\uparrow\uparrow i(2)r} & G_{k\alpha}^{\uparrow\downarrow i(2)r} \\ G_{k\alpha}^{\downarrow\uparrow i(2)r} & G_{k\alpha}^{\downarrow\downarrow i(2)r} \end{pmatrix} \quad (i = 1, 2, 3),$$

$$G_{k\alpha}^{\sigma'\sigma, 1(2)r}(t-t') = -i\theta(t-t') \langle \{a_{k\alpha\sigma'}(t) n_{\bar{\sigma}'}(t), c_{\sigma}^{\dagger}(t')\} \rangle,$$

$$G_{k\alpha}^{\sigma'\sigma, 2(2)r}(t-t') = -i\theta(t-t') \langle \{a_{k\alpha\bar{\sigma}'}^{\dagger}(t) c_{\sigma'}(t) c_{\bar{\sigma}'}(t), c_{\sigma}^{\dagger}(t')\} \rangle,$$

$$G_{k\alpha}^{\sigma'\sigma, 3(2)r}(t-t') = -i\theta(t-t') \langle \{a_{k\alpha\bar{\sigma}'}(t) c_{\bar{\sigma}'}^{\dagger}(t) c_{\sigma'}(t), c_{\sigma}^{\dagger}(t')\} \rangle.$$

$$g_{kL}^{r-1} G_{kL}^{1(2)r}(\varepsilon) = T_{kL} G^{(2)r}(\varepsilon) + \sum_{k'\alpha} [-T_{k'\alpha} G_{kLk'\alpha}^{1(3)r}(\varepsilon) + T_{k'\alpha}^* G_{kLk'\alpha}^{1(3)r}(\varepsilon)],$$

$$\tilde{g}_{kL}^{r-1} G_{kL}^{2(2)r}(\varepsilon) = T_{kL}^* G^{(2)r}(\varepsilon) + \sum_{k'\alpha} T_{k'\alpha}^* [G_{kLk'\alpha}^{3(3)r}(\varepsilon) + G_{kLk'\alpha}^{4(3)r}(\varepsilon)],$$

$$g_{kL}^{r-1} G_{kL}^{3(2)r}(\varepsilon) = T_{kL} [G^r(\varepsilon) - G^{(2)r}(\varepsilon)] + \sum_{k'\alpha} [-T_{k'\alpha} G_{kLk'\alpha}^{5(3)r}(\varepsilon) + T_{k'\alpha}^* G_{kLk'\alpha}^{6(3)r}(\varepsilon)],$$

$$\text{with } \tilde{g}_{k\alpha}^r(\varepsilon) = \begin{pmatrix} \tilde{g}_{k\alpha}^{\uparrow r}(\varepsilon) \\ \tilde{g}_{k\alpha}^{\downarrow r}(\varepsilon) \end{pmatrix} = \begin{pmatrix} \frac{1}{\varepsilon - 2\varepsilon_0 - U + \varepsilon_{k\alpha\downarrow} + i\eta} & \\ & \frac{1}{\varepsilon - 2\varepsilon_0 - U + \varepsilon_{k\alpha\uparrow} + i\eta} \end{pmatrix}, \quad g_{k\alpha}^r(\varepsilon) = \begin{pmatrix} g_{k\alpha}^{\downarrow r}(\varepsilon) \\ g_{k\alpha}^{\uparrow r, a}(\varepsilon) \end{pmatrix} = \begin{pmatrix} \frac{1}{\varepsilon - \varepsilon_{k\alpha\downarrow} + i\eta} & \\ & \frac{1}{\varepsilon - \varepsilon_{k\alpha\uparrow} + i\eta} \end{pmatrix}, \text{ and the third-order Green functions defined by:}$$

$$G_{kLk'\alpha}^{\sigma'\sigma, 1(3)r}(t-t') = -i\theta(t-t') \langle \{a_{kL\sigma'}(t) a_{k'\alpha\bar{\sigma}'}^{\dagger}(t) c_{\bar{\sigma}'}(t), c_{\sigma}^{\dagger}(t')\} \rangle,$$

$$G_{kLk'\alpha}^{\sigma'\sigma, 2(3)r}(t-t') = -i\theta(t-t') \langle \{a_{kL\sigma'}(t) c_{\bar{\sigma}'}^{\dagger}(t) a_{k'\alpha\bar{\sigma}'}(t), c_{\sigma}^{\dagger}(t')\} \rangle,$$

$$G_{kLk'\alpha}^{\sigma'\sigma, 3(3)r}(t-t') = -i\theta(t-t') \langle \{a_{kL\bar{\sigma}'}^{\dagger}(t) a_{k'\alpha\sigma'}(t) c_{\bar{\sigma}'}(t), c_{\sigma}^{\dagger}(t')\} \rangle,$$

$$G_{kLk'\alpha}^{\sigma'\sigma, 4(3)r}(t-t') = -i\theta(t-t') \langle \{a_{kL\bar{\sigma}'}^{\dagger}(t) c_{\sigma'}(t) a_{k'\alpha\bar{\sigma}'}(t), c_{\sigma}^{\dagger}(t')\} \rangle,$$

$$G_{kLk'\alpha}^{\sigma'\sigma, 5(3)r}(t-t') = -i\theta(t-t') \langle \{a_{kL\bar{\sigma}'}(t) a_{k'\alpha\bar{\sigma}'}^{\dagger}(t) c_{\sigma'}(t), c_{\sigma}^{\dagger}(t')\} \rangle,$$

$$G_{kLk'\alpha}^{\sigma'\sigma, 6(3)r}(t-t') = -i\theta(t-t') \langle \{a_{kL\bar{\sigma}'}(t) c_{\bar{\sigma}'}^{\dagger}(t) a_{k'\alpha\sigma'}(t), c_{\sigma}^{\dagger}(t')\} \rangle.$$

It is worthily mentioning that one usually takes the Hatree-Fock decoupling approximation up to the second-order for Green functions in most systems. Such a decoupling scheme is not adequate for the present single-level QD σ coupled system, as it could smear some characteristic features that come from electronic correlations. In order to extract more information from the many-body interactions, we should consider the equation of motion up to the third-order of Green functions $G_{k\alpha}^{i(2)r}(\varepsilon)$ in Eq. (15). In above derivations, we have invoked the following decoupling approximations for Green functions[41]: $G_{kLk'\alpha}^{\sigma'\sigma, 1(3)r}(\varepsilon) =$

$G_{kLk'\alpha}^{\sigma'\sigma,2(3)r}(\varepsilon) = G_{kLk'\alpha}^{\sigma'\sigma,3(3)r}(\varepsilon) = G_{kLk'\alpha}^{\sigma'\sigma,6(3)r}(\varepsilon) = 0$, $G_{kLk'\alpha}^{\sigma'\sigma,4(3)r}(\varepsilon) = -\delta_{kL,k'\alpha}f_L(\varepsilon_{kL\bar{\sigma}'})G^{\sigma'\sigma,r}(\varepsilon)$,
 $G_{kLk'\alpha}^{\sigma'\sigma,5(3)r}(\varepsilon) = \delta_{kL,k'\alpha}[1 - f_L(\varepsilon_{kL\bar{\sigma}'})]G^{\sigma'\sigma,r}(\varepsilon)$. As we ignore the spin-flip scatterings in the present system, the off-diagonal elements associated with different spins of the third-order Green function are sent to zero, namely, the higher-order spin correlations in the ferromagnetic leads are neglected.

With these results, we may obtain

$$\begin{aligned}
 G_{kL}^{1(2)r}(\varepsilon) &= T_{kL}g_{kL}G^{(2)r}(\varepsilon), \\
 G_{k,q}^{2(2)r}(\varepsilon) &= T_{kL}^*\tilde{g}_{k\alpha}^r[G^{(2)r}(\varepsilon) - \bar{F}_L G^r(\varepsilon)], \\
 G_{k,q}^{3(2)r}(\varepsilon) &= -T_{kL}g_{k\alpha}^r[G^{(2)r}(\varepsilon) - \bar{F}_L G^r(\varepsilon)],
 \end{aligned}$$

with $F_\alpha = \begin{pmatrix} f_\alpha(\varepsilon_{k\alpha\uparrow}) \\ f_\alpha(\varepsilon_{k\alpha\downarrow}) \end{pmatrix}$ and $\bar{F}_\alpha = \begin{pmatrix} f_\alpha(\varepsilon_{k\alpha\downarrow}) \\ f_\alpha(\varepsilon_{k\alpha\uparrow}) \end{pmatrix}$.

Similarly, a more straightforward but somewhat complicated calculation gives rise to the following equations

$$\begin{aligned}
 G_{kR}^{1(2)r}(\varepsilon) &= \frac{1}{2}T_{kR}\sin\theta[f_R(\varepsilon_{kR\uparrow})g_{kR}^{\uparrow r}(\varepsilon) - f_R(\varepsilon_{kR\downarrow})g_{kR}^{\downarrow r}(\varepsilon)]\hat{\sigma}_1 G^r(\varepsilon) \\
 &+ T_{kR}\left[\cos^2\frac{\theta}{2}g_{kR}^r(\varepsilon) + \sin^2\frac{\theta}{2}g_{kR}^r(\varepsilon)\right]G_{q,q}^{(2)r}(\varepsilon)
 \end{aligned} \tag{16}$$

$$\begin{aligned}
 G_{kR}^{2(2)r}(\varepsilon) &= \frac{1}{2}T_{kR}\sin\theta[\tilde{g}_{kR}^{\downarrow,r}(\varepsilon)f_R(\varepsilon_{kR\uparrow}) - \tilde{g}_{kR}^{\uparrow,r}(\varepsilon)f_R(\varepsilon_{kR\downarrow})]\hat{\sigma}_1 G^r(\varepsilon) \\
 &- T_{kR}\left[\cos^2\frac{\theta}{2}\tilde{g}_{kR}^r(\varepsilon)\bar{F}_R + \sin^2\frac{\theta}{2}\tilde{g}_{kR}^r(\varepsilon)F_R\right]G^r(\varepsilon) \\
 &+ \frac{1}{2}T_{kR}\sin\theta[\tilde{g}_{kR}^{\uparrow,r}(\varepsilon) - \tilde{g}_{kR}^{\downarrow,r}(\varepsilon)]\hat{\sigma}_1 G^{(2)r}(\varepsilon) \\
 &+ T_{kR}\left[\cos^2\frac{\theta}{2}\tilde{g}_{kR}^r(\varepsilon) + \sin^2\frac{\theta}{2}\tilde{g}_{kR}^r(\varepsilon)\right]G^{(2)r}(\varepsilon),
 \end{aligned} \tag{17}$$

$$\begin{aligned}
 G_{kR}^{3(2)r}(\varepsilon) &= -T_{kR}^*\left[\sin^2\frac{\theta}{2}g_{kR}^r(\varepsilon) + \cos^2\frac{\theta}{2}g_{kR}^r(\varepsilon)\right]G^{(2)r}(\varepsilon) \\
 &+ T_{kR}^*\left[\sin^2\frac{\theta}{2}g_{kR}^r(\varepsilon)F_R + \cos^2\frac{\theta}{2}g_{kR}^r(\varepsilon)\bar{F}_R\right]G^r(\varepsilon),
 \end{aligned} \tag{18}$$

where $\hat{\sigma}_1 = \begin{pmatrix} 0 & 1 \\ 1 & 0 \end{pmatrix}$, and $\tilde{g}_{k\alpha}^r(\varepsilon) = \begin{pmatrix} \tilde{g}_{k\alpha}^{\downarrow r}(\varepsilon) \\ \tilde{g}_{k\alpha}^{\uparrow r}(\varepsilon) \end{pmatrix} = \begin{pmatrix} \frac{1}{\varepsilon - 2\varepsilon_0 - U + \varepsilon_{k\alpha\uparrow} + i\eta} \\ \frac{1}{\varepsilon - 2\varepsilon_0 - U + \varepsilon_{k\alpha\downarrow} + i\eta} \end{pmatrix}$.

On the other hand, the second-order retarded Green's function can be expressed as of the following form

$$W_1 G^{(2)r}(\varepsilon) = N + W_2 G^r(\varepsilon), \quad (19)$$

where

$$\begin{aligned} W_1 = & (\varepsilon - \varepsilon_0 - U) - \sum_{kL} T_{kL} T_{kL}^* g_{kL}^r(\varepsilon) - \sum_{kL} T_{kL} T_{kL}^* \tilde{g}_{kL}^r(\varepsilon) - \sum_{kL} T_{kL} T_{kL}^* g_{\bar{k}L}^r(\varepsilon) \\ & - \sum_{kR} T_{kR} T_{kR}^* \left[\cos^2 \frac{\theta}{2} g_{kR}^r(\varepsilon) + \sin^2 \frac{\theta}{2} g_{\bar{k}R}^r(\varepsilon) \right] \\ & - \sum_{kR} T_{kR} T_{kR}^* \frac{1}{2} \sin \theta \left[\tilde{g}_{kR}^{\uparrow,r}(\varepsilon) - \tilde{g}_{kR}^{\downarrow,r}(\varepsilon) \right] \hat{\sigma}_1 \\ & - \sum_{kR} T_{kR} T_{kR}^* \left[\cos^2 \frac{\theta}{2} \tilde{g}_{kR}^r(\varepsilon) + \sin^2 \frac{\theta}{2} \tilde{g}_{\bar{k}R}^r(\varepsilon) \right] \\ & - \sum_{kR} T_{kR} T_{kR}^* \left[\cos^2 \frac{\theta}{2} g_{kR}^r(\varepsilon) + \sin^2 \frac{\theta}{2} g_{\bar{k}R}^r(\varepsilon) \right], \end{aligned}$$

$$\begin{aligned} W_2 = & - \sum_{kL} T_{kL} T_{kL}^* \tilde{g}_{kL}^r(\varepsilon) \bar{F}_L - \sum_{kL} T_{kL} T_{kL}^* g_{kL}^r(\varepsilon) \bar{F}_L \\ & + \sum_{kR} T_{kR} T_{kR}^* \frac{1}{2} \sin \theta [g_{kR}^{\uparrow,r}(\varepsilon) f_R(\varepsilon_{kR\uparrow}) - g_{kR}^{\downarrow,r}(\varepsilon) f_R(\varepsilon_{kR\downarrow})] \hat{\sigma}_1 \\ & + \sum_{kR} T_{kR} T_{kR}^* \frac{1}{2} \sin \theta [\tilde{g}_{kR}^{\downarrow,r}(\varepsilon) f_R(\varepsilon_{kR\uparrow}) - \tilde{g}_{kR}^{\uparrow,r}(\varepsilon) f_R(\varepsilon_{kR\downarrow})] \hat{\sigma}_1 \\ & - \sum_{kR} T_{kR} T_{kR}^* \left[\cos^2 \frac{\theta}{2} \tilde{g}_{kR}^r(\varepsilon) \bar{F}_R + \sin^2 \frac{\theta}{2} \tilde{g}_{\bar{k}R}^r(\varepsilon) F_R \right] \\ & - \sum_{kR} T_{kR} T_{kR}^* \left[\cos^2 \frac{\theta}{2} g_{kR}^r(\varepsilon) \bar{F}_R + \sin^2 \frac{\theta}{2} g_{\bar{k}R}^r(\varepsilon) F_R \right]. \end{aligned}$$

By combining Eq. (19) with Eq. (15), we get

$$(\varepsilon - \varepsilon_0 - \Sigma_0^r - U W_1^{-1} W_2) G^r = \mathbf{1} + U W_1^{-1} N. \quad (20)$$

From this equation, the retarded Green function G^r can be obtained. We would like to point out that the averaged values involved in Eq. (15) should be obtained self-consistently by

$$\begin{aligned} \langle n_\sigma \rangle &= \Im m \int \frac{d\varepsilon}{2\pi} G^{\sigma\sigma<}(\varepsilon), \\ \langle c_\sigma^\dagger c_{\bar{\sigma}} \rangle &= -i \int \frac{d\varepsilon}{2\pi} G^{\bar{\sigma}\sigma<}(\varepsilon). \end{aligned}$$

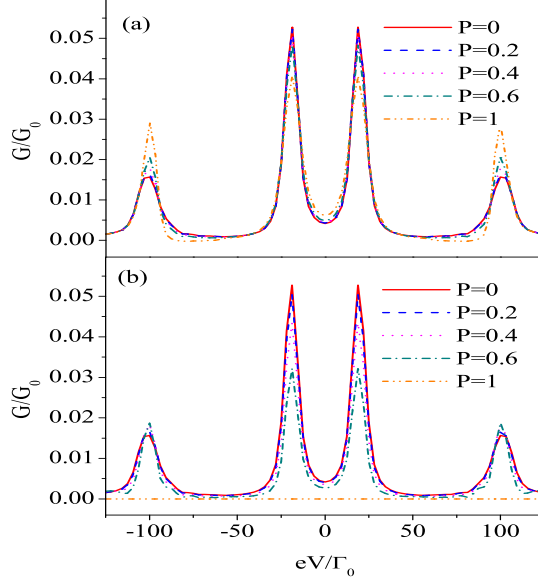


FIG. 2: The bias dependence of the differential conductance G for different polarization P in parallel (a) and antiparallel (b) configurations of magnetizations. The parameters are taken as $\varepsilon_0 = 10\Gamma_0$, $U = 40\Gamma_0$, $k_B T = 0.3\Gamma_0$.

These above-mentioned equations establish the fundamental basis for numerically investigating the spin-dependent transport properties of the FM-QD-FM coupled MTJs.

III. NUMERICAL RESULTS

Without losing the generality, in the following numerical calculations we may further suppose that the two ferromagnets are made of the same materials, i.e., $P_L = P_R = P$, where $P_{L(R)} = (\Gamma_{L(R)\uparrow} - \Gamma_{L(R)\downarrow}) / (\Gamma_{L(R)\uparrow} + \Gamma_{L(R)\downarrow})$ is the polarization of the left (right) ferromagnet. Then, we can introduce $\Gamma_{L\uparrow,\downarrow} = \Gamma_{R\uparrow,\downarrow} = \Gamma_0(1 \pm P)$, where $\Gamma_0 = \Gamma_{L(R)\uparrow}(P = 0) = \Gamma_{L(R)\downarrow}(P = 0)$ will be taken as an energy scale. The tunnel matrix elements $T_{kL(R)}$ is presumed to take values at the Fermi level. We will take $I_0 = \frac{e\Gamma_0}{h}$ and $G_0 = \frac{e^2}{h}$ as scales for the currents and corresponding differential conductance, respectively.

A. Differential conductance

The bias dependences of the tunnel electrical current and the differential conductance $G = \frac{dI}{dV}$ in the FM-QD-FM coupled system have been reexamined within the present scheme. It is found that the tunnel electrical current exhibits two-step features, which corresponds to the resonant tunneling of electrons through the QD at energy levels ε_0 and $\varepsilon_0 + U$. The corresponding differential conductance as a function of the bias thus exhibits resonant peaks, where the large peak at a lower voltage corresponds to the discrete level ε_0 , and a small resonant peak corresponds to the level $\varepsilon_0 + U$. It is uncovered that with the increase of the interaction U , the peaks of $G(V)$ corresponding to the discrete level $\varepsilon_0 + U$ shift towards the higher voltage side without changing the peak amplitude for both parallel and antiparallel configurations. This is because an increase of U makes two discrete levels ε_0 and $\varepsilon_0 + U$ become far apart, thereby leading to that the resonant positions of main and charging peaks of $G(V)$ are far separated. These observations are quite consistent with the previous studies (see e.g. Ref.[35]).

The bias dependence of the differential conductance for different polarizations in the parallel and antiparallel configurations of magnetization is shown in Fig. 2. It can be found that in the parallel configuration there is only slight changes for different polarizations except for $P = 1$, as displayed in Fig. 2(a). We can understand this property from the point of view of the resonant tunneling through two barriers[31], namely, the two barriers are of the same height, and the resonant probability is unity in this case, that is independent with P . The small changes with P observed in Fig. 2(a) is caused by the interaction U . However, it is quite different for the case with full polarization $P = 1$, which comes from the fact that the conductance for $P = 1$ has only one channel. It is interesting to note that with increasing P in the case of parallel alignment, although the main peaks at the bias corresponding to the energy level ε_0 are suppressed, the charging peaks at the bias corresponding to the level $\varepsilon_0 + U$ are enhanced. In this case, more electrons from the left enter into the QD through the channel $\varepsilon_0 + U$ to tunnel into the right lead. For the antiparallel configuration, it can be seen that the main peaks of the conductance decrease as the polarization P increases, while the charging peaks remain almost intact, as shown in Fig. 2(b), that is different from the case of parallel configuration, and is due to the conventional spin-valve effect in MTJs. For $P = 1$, the conductance becomes zero, which is nothing but a perfect spin-valve effect.

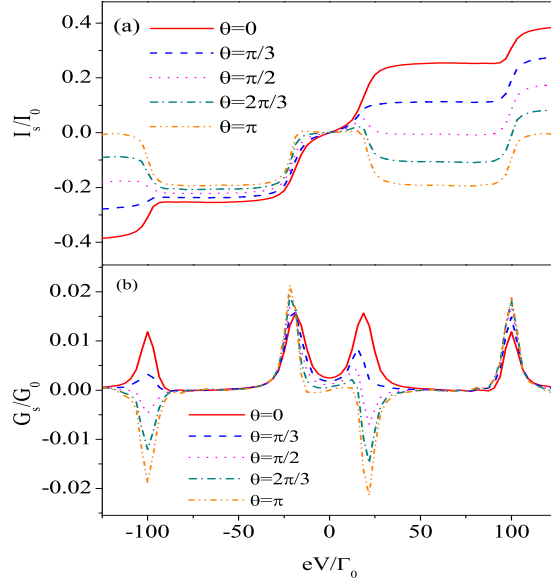


FIG. 3: The bias dependence of the spin current I_s (a) and spin differential conductance G_s (b) for different angle θ at $P = 0.4$. The other parameters are taken the same as in Fig. 2.

B. Spin current and spin differential conductance

The bias dependence of the spin current I_s and its corresponding spin differential conductance defined by $G_s = \frac{dI_s}{dV}$ for different angles is shown in Fig. 3. It can be seen that, by changing the relative angle θ , the spin current can change its magnitude even its sign. At $V > 0$, when $\theta < \pi/2$, the spin current I_s shows step-like behaviors, and $I_s > 0$; while for $\theta > \pi/2$, I_s exhibits behaviors similar to a basin-like shape, and $I_s < 0$ at the bottom of the "basin". This shows that the effect of the relative orientation of magnetizations on the spin current is more obvious. At two resonant positions corresponding to levels ε_0 and $\varepsilon_0 + U$, I_s begins to sharply change. It is clearly seen in Fig. 3(b) that at $V > 0$, the spin conductance shows sharp resonant peaks and dips at the levels ε_0 and $\varepsilon_0 + U$, although for $\theta = 0$ and $\pi/3$ the resonance corresponding to ε_0 shows a peak, while for $\theta = \pi/2, 2\pi/3$ and π the first resonance shows a sharp dip. The resonances corresponding to the level $\varepsilon_0 + U$ exhibit peaks for all θ . At $\theta = 0$, the two resonant peaks of I_s have comparable weights; at $\theta = \pi/3$, the first peak has a small weight, while the second peak has a large weight; at $\theta = \pi/2$, the first dip of I_s has a small amplitude, while the other peak has a large amplitude; at $\theta = 2\pi/3$, the resonant dip and peak have almost the same amplitude; and at $\theta = \pi$, the first dip has

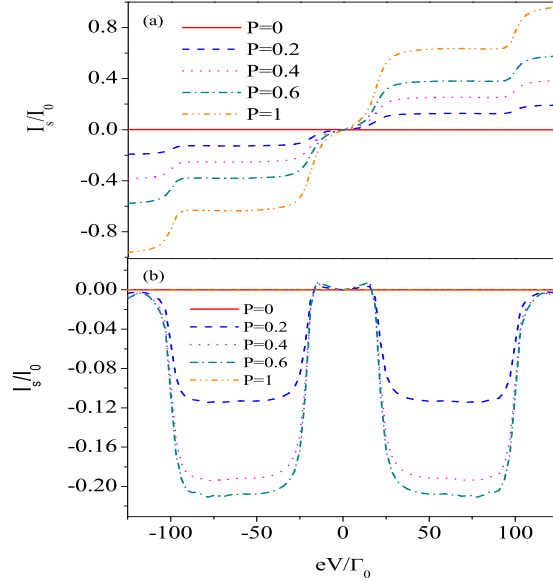


FIG. 4: The bias dependence of the spin current I_s for different polarization P in parallel (a) and antiparallel (b) configurations of magnetizations. The other parameters are taken the same as in Fig. 2.

a larger amplitude than the peak. Evidently, the spin current and spin conductance have no spin-valve effect, showing that the spin current and spin conductance have quite different characteristics from their electrical counterparts.

The step-like and basin-like behaviors of the bias dependence of the spin current for different polarizations in parallel and antiparallel configurations are presented in Figs. 4(a) and (b), respectively. For $P = 0$, as there is no polarization in electrodes, the contribution of electrons with spin up is the same as that of spin down, leading to the spin current vanishes. In the case of parallel alignment ($\theta = 0$), with increasing the polarization P , the contribution of spin up is increased while that of spin down is decreased, thus resulting in the magnitude of the spin current increased, as shown in Fig. 4(a). The step-like behavior of I_s against V comes from the resonant tunneling. The situation becomes a bit complicated in the case of antiparallel alignment ($\theta = \pi$). When $P = 0$ and 1, the spin current is zero, because for the former $I_{\uparrow} = I_{\downarrow}$ while for the latter $I_{\uparrow} = I_{\downarrow} = 0$, as shown in Fig. 4(b). For $P \neq 0$ and 1, with increasing the bias voltage the spin current decreases steeply at the resonant position corresponding to the QD energy level ε_0 , and then keeps a constant until the other resonant

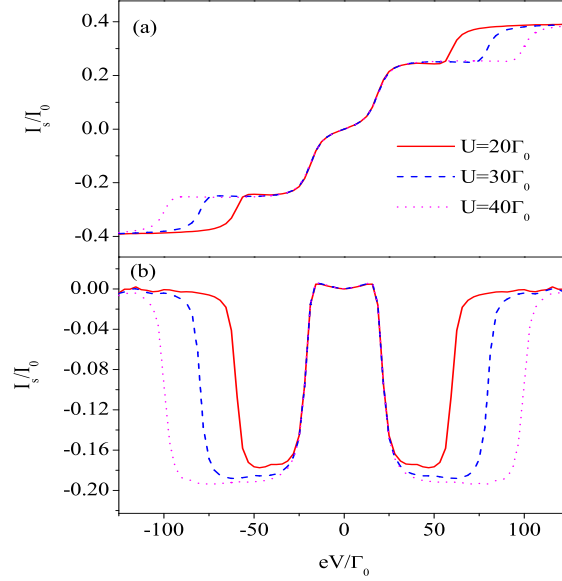


FIG. 5: The bias dependence of spin current I_s in parallel (a) and antiparallel (b) configurations for different Coulomb interaction U , where $P = 0.4$, and the other parameters are taken the same as in Fig. 2.

position corresponding to the level $\varepsilon_0 + U$ where I_s increases sharply, leading to the spin current shows a basin-like behavior. The larger the polarization P ($\neq 0, 1$), the deeper the bottom of the basin. These results demonstrate that the spin current I_s has quite different behaviors in parallel and antiparallel configurations.

Fig. 5 shows the bias dependence of spin current in collinear configurations for different Coulomb interaction U . It can be found that the overall qualitative behavior of I_s against V looks similar to that shown in Fig. 4. With increasing U , in the parallel alignment the second plateau of the spin current I_s becomes wider, as shown in Fig. 5(a); while in the antiparallel alignment apart from that the bottom of the "basin" becomes deeper, the width of the "basin" also becomes wider, as shown in Fig. 5(b). This is again from the fact that an increase of U makes the resonant positions corresponding QD discrete levels ε_0 and $\varepsilon_0 + U$ become far separated.

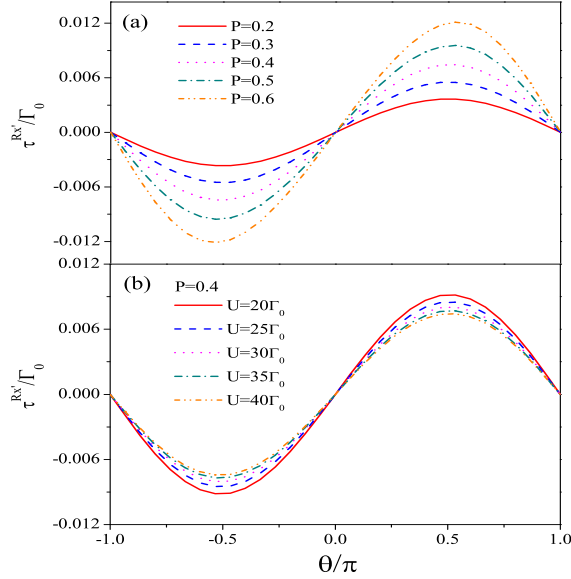


FIG. 6: The current-induced spin transfer torque against the relative orientation angle θ for different polarization P (a) and different interaction U (b) at the bias voltage $V = 25\Gamma_0/e$. The other parameters are taken the same as in Fig. 2.

C. Current-induced spin transfer torque

The angular dependence of the CISTT for different polarization and Coulomb interaction is shown in Fig. 6. It is seen that the CISTT versus the angle θ shows a sine-like behavior, consistent with the finding in Ref.[42]. At $\theta = 0$ and π , i.e., the magnetizations of the two ferromagnetic electrodes are collinearly aligned, the CISTT vanishes, which is obvious as the spin torque $\propto \mathbf{S}_R \times (\mathbf{S}_L \times \mathbf{S}_R)$, where \mathbf{S}_L and \mathbf{S}_R are the spin moments of the left and right ferromagnets. With increasing the polarization P , the magnitude of the CISTT is enhanced, as displayed in Fig. 6(a). This is in agreement with the statement that the torque is proportional to the polarization of the other ferromagnet[42]. With the increase of Coulomb interaction U , the magnitude of the CISTT is decreased, as seen in Fig. 6(b). This can be understood in such a way that the contribution of the tunneling through the discrete level $\varepsilon_0 + U$ is decreased with increasing the interaction U , thus leading to a decrease of the spin transfer torque.

The bias dependences of the CISTT for different polarizations and Coulomb interactions at a given angle $\theta = \pi/3$ are shown in Figs. 7(a) and (b). It is seen that with increasing the

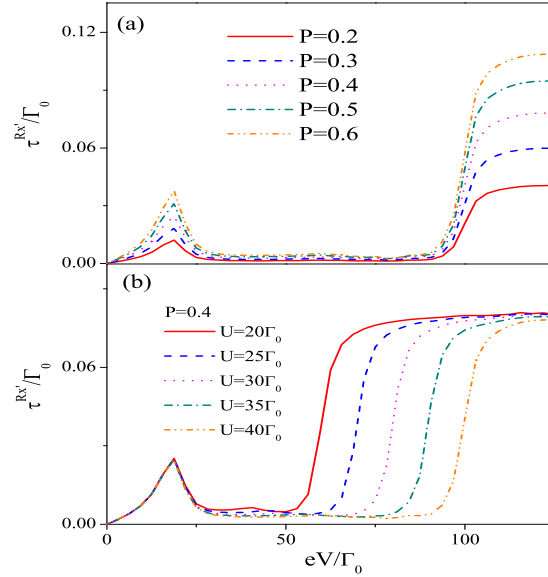


FIG. 7: The bias dependence of the current-induced spin transfer torque for different polarization P (a) and U (b) at $\theta = \pi/3$. The other parameters are taken the same as in Fig. 2.

bias voltage, the CISTT first increases slowly to a sharp peak, then decreases dramatically to almost zero, and after undergoing a wider flat, it increases suddenly to another plateau. The position of the first sharp peak in the curve of CISTT versus V is observed to be independent of the polarization as well as the Coulomb interaction, showing that it is a resonant peak at the resonant position ε_0 . The second sharp increase of the CISTT against V is also from the resonance at the QD discrete energy level $\varepsilon_0 + U$. From Fig. 7(a), one may find that with increasing the polarization the magnitudes of the CISTT at the two resonant positions increase. This is because the transmission coefficient of electrons is proportional to the polarization[33], while the CISTT depends on the tunneling electrical current that is determined by the transmission coefficient. Thus, an increase of polarization would enhance the CISTT at the resonant positions. The effect of the Coulomb interaction U on the CISTT is shown in Fig. 7(b). At the first peak, it is independent of U , suggesting that it is a resonance at the level ε_0 ; while with increasing U , the second resonant positions move to higher voltages, showing that the second resonance takes place at the level $\varepsilon_0 + U$. It is interesting to note that at a given polarization the CISTT goes to a saturation plateau at the bias larger than $(\varepsilon_0 + U)/e$, which is independent of the Coulomb interaction. From

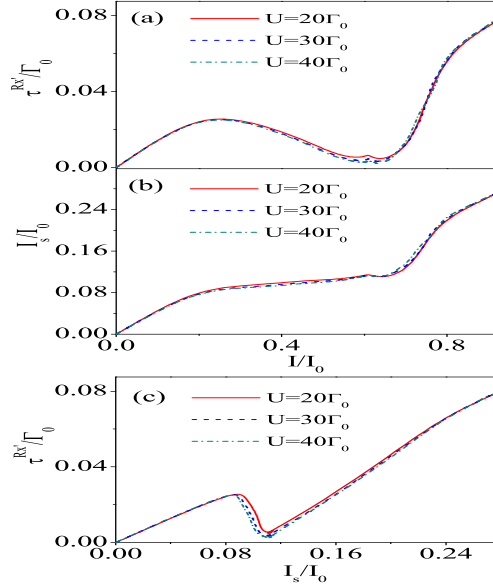


FIG. 8: The current-induced spin transfer torque (a) and the spin current (b) against the electrical current as well as the current-induced spin transfer torque versus the spin current (c) for different U at $\theta = \pi/3$ and $P = 0.4$. The other parameters are taken the same as in Fig. 2.

Fig. 7, we could see that the CISTT can be remarkably enhanced at the QD discrete energy levels which may be adjusted by changing the gate voltage.

What is the relationship between the CISTT, the electrical current and the spin current in this FM-QD-FM coupled system? The answer is presented in Fig. 8 for different U at $\theta = \pi/3$. With increasing the electrical current, the CISTT goes up linearly to a round peak, then decreases slowly to a broad minimum, and then increases sharply, as shown in Fig. 8(a). The first round peak is owing to the resonant tunneling at the level ε_0 ; while the second sharp increase is caused by the resonant tunneling at the level $\varepsilon_0 + U$. The spin current I_s is found to increase non-monotonically with increasing the electrical current I , as illustrated in Fig. 8(b). This is quite different from the spin current in FM-SC-FM tunnel junctions where the spin current is proportional to the injection current[43]. In the curves of I_s against I , the two resonances can be clearly seen. The CISTT as a function of I_s shows a kink-like behavior, as displayed in Fig. 8(c). With increasing I_s , the CISTT first shows a linear behavior, then suddenly drops to nearly zero, and then increases almost linearly again. This kink-like behavior is caused by the resonant tunneling at the levels ε_0

and $\varepsilon_0 + U$, which manifests the same thing as in Fig. 7. Away from the kink, the CISTT appears to be proportional to the spin current. The reason is that the electrons with opposite spins from the left ferromagnetic electrode entering into the right electrode exert the torques with opposite directions on the spins of the right electrode, giving rise to that the magnitude of the CISTT is determined by the difference between the magnitudes of torques exerted by electrons with spin up and spin down. Considering that the spin current is defined by the difference between the electrical currents of spin up and spin down, while the spin transfer torque is proportional to the electrical current [6, 7], the proportionality between the CISTT and the spin current is conceivable. It is seen that for different U the curves in Fig. 8 are almost unchanged, showing that the Coulomb interaction has less effect on the CISTT versus I and I_s , as well as I_s versus I . This is because the Coulomb interaction U only changes the resonant positions.

IV. SUMMARY

We have investigated the spin-dependent transport properties in a FM-QD-FM coupled system by means of the nonequilibrium Green functions. It has been found that by changing the relative orientation of both magnetizations, the spin current can change its magnitude even its sign. For positive bias voltages, when the relative orientation angle is less than $\pi/2$, the spin current shows a step-like behavior, and the spin current is positive; when the relative orientation angle is greater than $\pi/2$, the spin current behaviors similar to a basin-like shape, and is negative at the bottom of the "basin". With increasing the Coulomb interaction U in the QD, it has been uncovered that the resonant positions for the tunneling electrical current and spin current become far separated. The CISTT is observed to first increase slowly to a sharp peak with increasing the bias voltage, then decrease dramatically to almost zero; and after undergoing an unchanged stage, it increases suddenly to another plateau. Such a behavior is obviously resulted from the resonant tunneling through the central QD. The magnitudes of the CISTT at two resonant positions are observed to increase with increasing the polarization of the ferromagnet. At the bias larger than $(\varepsilon_0 + U)/e$, the CISTT is seen to reach a saturation plateau which is independent of the Coulomb interaction. In addition, it has been demonstrated that the CISTT as a function of the spin current shows a kink-like behavior, and away from the kink, the CISTT increases almost linearly with increasing the

spin current. The CISTT as a function of the electrical current shows a non-monotonic behavior, while the spin current is found to be nonlinearly proportional to the electrical current. Besides, the Coulomb interaction is shown to have less effect on the behaviors of the CISTT as functions of the tunneling electrical current and spin current, as well as the spin current as a function of the electrical current.

Finally, we would like to mention that the CISTT can be greatly enhanced when the bias voltage meets with the discrete levels of the QD at two resonant positions. While the energy level of the QD can be adjusted by tuning the gate voltage, the resonant property of the CISTT offers an alternative premise to develop a spintronic device through the current-controlled magnetization reversal effect.

Acknowledgments

We have benefitted from discussions with B. Jin, Z. C. Wang, and Z. G. Zhu. This work is supported in part by the National Science Foundation of China (Grants Nos. 90403036, 20490210, 10247002) and by the Chinese Academy of Sciences.

[] *Corresponding author. E-mail: gsu@gucas.ac.cn.

- [1] G. A. Prinz, *Science* **282**, 1660 (1998).
- [2] S. A. Wolf, D. D. Awschalom, R. A. Buhrman, J. M. Daughton, S. von Molnár, M. L. Roukes, A. Y. Chtchelkanova, and D. M. Treger, *Science* **294**, 1488 (2001).
- [3] I. Žutić, J. Fabian and S. D. Sarma, *Rev. Mod. Phys.* **76**, 323 (2004).
- [4] S. Maekawa, *J. Magn. Magn. Mater.* **272-276**, e1459 (2004).
- [5] G. Su, in *Progress in Ferromagnetism Research*, edited by V. N. Murray (Nova Science Publishers, Inc., New York, 2005), pp. 85-123.
- [6] J. C. Slonczewski, *J. Magn. Magn. Mater.* **159**, L1 (1996).
- [7] L. Berger, *Phys. Rev. B* **54**, 9353 (1996).
- [8] L. Berger, *J. Appl. Phys.* **91**, 6795 (2002).
- [9] M. Tsoi, A. G. M. Jansen, J. Bass, W.-C. Chiang, M. Seck, V. Tsoi, and P. Wyder, *Phys. Rev. Lett.* **80**, 4281 (1998).

- [10] E. B. Myers, D. C. Ralph, J. A. Katine, R. N. Louie and R. A. Buhrman, *Science* **285**, 867 (1999).
- [11] J. A. Katine, F. J. Albert, R. A. Buhrman, E. B. Myers and D. C. Ralph, *Phys. Rev. Lett.* **84**, 3149 (2000).
- [12] J. E. Wegrowe, D. Kelly, Y. Jaccard, P. Guittienne, and J. P. Ansermet, *Europhys. Lett.* **45**, 626 (1999).
- [13] J. Z. Sun, *J. Magn. Magn. Mater.* **202**, 157 (1999).
- [14] A. Asamitsu, Y. Tomioka, H. Kuwahara and Y. Tokura, *Nature* **388**, 50 (1997).
- [15] X. Waintal, E. B. Myers, P. W. Brouwer and D. C. Ralph, *Phys. Rev. B* **62**, 12317 (2000).
- [16] A. Bratass, Yu. V. Nazarov, G. E. W. Bauer, *Eur. Phys. J. B* **22**, 99 (2001).
- [17] Z. G. Zhu, G. Su, B. Jin, Q. R. Zheng, *Phys. Rev. B* **68**, 224413 (2003); *Phys. Lett. A* **306**, 249 (2003).
- [18] Y. Tserkovnyak and A. Brataas, *Phys. Rev. B* **65**, 094517 (2002).
- [19] X. Waintal and P. W. Brouwer, *Phys. Rev. B* **63**, 220407 (2001).
- [20] X. Waintal and P. W. Brouwer, *Phys. Rev. B* **65**, 054407 (2002).
- [21] H. F. Mu, Q. R. Zheng, B. Jin, G. Su, *Phys. Lett. A* **336**, 66 (2005).
- [22] X. Waintal and O. Parcollet, *Phys. Rev. Lett* **94**, 247206 (2005).
- [23] H. F. Mu, G. Su, Q. R. Zheng and B. Jin, *Phys. Rev. B* **71**, 064412 (2005); B. Jin, G. Su, Q. R. Zheng, *Phys. Rev. B* **71**, 144514 (2005).
- [24] W. Rudziński and J. Barnaś, *Phys. Rev. B* **64**, 085318, (2001).
- [25] J. Fransson, O. Eriksson, I. Sandalov, *Phys. Rev. Lett.* **88**, 226601, (2002).
- [26] P. Zhang, Q. K. Xue, Y. P. Wang, and X. C. Xie, *Phys. Rev. Lett.* **89**, 286803 (2002).
- [27] B. R. Bulka, S. Lipiński, *Phys. Rev. B* **67**, 024404 (2003).
- [28] R. López, D. Sánchez, *Phys. Rev. Lett.* **90**, 116602 (2003).
- [29] J. Martinek, Y. Utsumi, H. Imamura, J. Barnaś, S. Maekawa, J. König, G. Schön, *Phys. Rev. Lett.* **91**, 127203 (2003).
- [30] J. N. Pedersen, J. Q. Thomassen, and K. Flensberg, *Phys. Rev. B* **72**, 045341 (2005).
- [31] N. Sergueev, Q. F. Sun, H. Guo, B. G. Wang, and J. Wang, *Phys. Rev. B* **65**, 165303 (2002).
- [32] J. König, J. Martinek, *Phys. Rev. Lett.* **90**, 166602 (2003).
- [33] Z. G. Zhu, G. Su, Q. R. Zheng and B. Jin, *Phys. Rev. B* **70**, 174403 (2004).
- [34] M. Braun, J. König and J. Martinek, *Phys. Rev. B* **70**, 195345 (2004).

- [35] W. Rudziński, J. Barnaś, R. Świrkwicz, M. Wilczyński, Phys. Rev. B **71**, 205307 (2005).
- [36] W. Wetzels, G. E. W. Bauer, Phys. Rev. B **72**, 020407 (2005).
- [37] J. Fransson, Europhys. Lett. **70**, 796 (2005).
- [38] J. Fransson, Phys. Rev. B **72**, 045415 (2005).
- [39] I. Weymann, J. Barnaś, Eur. Phys. J. B **46**, 289 (2005).
- [40] T. K. Ng, Phys. Rev. Lett. **76**, 487 (1996).
- [41] H. Haug and A. P. Jauho, *Quantum Kinetics in Transport and Optics of Semiconductors* (Springer, Berlin, 1998).
- [42] J. C. Slonczewski, Phys. Rev. B **71**, 024411 (2005).
- [43] S. Takahashi, H. Imamura, S. Maekawa, Physica C **341-348**, 1515 (2000).